

Enhanced signal response in globally coupled networks of bistable oscillators: Effects of mean field density and signal shape

Frank Thomas Ndjomatchoua ^{1,*}, Carlos Lawrence Gninzanlong,¹ Thierry Landry Michel Mbong Djomo,² Maxime Fabrice Pebeu Kepnang,¹ and Clément Tchawoua¹

¹*Department of Physics, Faculty of Science, University of Yaoundé 1, P.O. Box 812, Ngoa Ekelle, Yaoundé, Cameroon*

²*Department of Civil Engineering, National Higher Polytechnic Institute, University of Bamenda, P.O. Box 39, Bambili, Bamenda, Cameroon*



(Received 20 December 2022; revised 7 May 2023; accepted 2 June 2023; published 16 June 2023)

This paper studies a set of globally coupled bistable oscillators, all subjected to the same weak periodic signal and identical coupling. The effect of mean field density (MFD) on global dynamics is analyzed. The oscillators switch from intra- to interwell motion as MFD increases, clearly demonstrating MFD-enhanced signal amplification. A maximum amplification also occurs at a moderate level of MFD, indicating that the response exhibits a nonmonotonic sensitivity to MFD. The MFD-enhanced response depends mainly on the signal intensity but not on the signal frequency or the network topology. The analytical investigation provides a simplified model to study the mechanism underlying this resonancelike behavior. It is shown that by modifying the bistability nature of the potential energy, the mean field density can promote well-to-well oscillations and larger amplitude motions. Finally, the robustness of this phenomenon to various signal waveforms is examined. It can therefore be used alternatively to efficiently amplify weak signals in practical situations with large network sizes.

DOI: [10.1103/PhysRevE.107.064208](https://doi.org/10.1103/PhysRevE.107.064208)

I. INTRODUCTION

Improving the response of a system to a weak input signal is important in several areas of science and engineering, such as sensory information processing and perception [1], weak machine fault detection [2], and the transmission of weak electrical [3], optimization of low-power harvesting [4], or all-photonic/phononic transistors [5,6].

Various approaches have been developed to improve the detection or amplification of external signals in coupled nonlinear oscillators. Among others, vibrational resonance [7], nonlinear supratransmission [8], or a single impurity [9] can be used. Optimal heterogeneity in system parameters [10,11] and phase disorder [12] can amplify weak signals in a resonancelike manner.

The characteristics of the coupling are also crucial in observing this phenomenon. To illustrate, unidirectional coupling enhances the response to a weak periodic signal [13–16]. For any value of coupling, Acebrón *et al.* [17] observed no enhancement of the external signal in all-to-all networks. This observation has been further corroborated by studies investigating the effect of coupling diversity between oscillators, e.g., random scale-free or interactive-repulsive interactions [17,18], couplings with heterogeneous signs or strengths [19,20]. It is suggested that the diversity in the coupling of oscillators promotes a competition-induced resonance effect, where networks with identical couplings cannot [17–20].

In contrast to previous investigations [7–14,16–20], the present paper aims to show that weak signal enhancement is observed in a resonancelike manner for identically and globally (all-to-all) coupled oscillators. This coupling topology is simple, analytically tractable, and widely used in the literature on similar topics [7–14,16–20]. For comparison purposes, two other topologies such as star and nearest-neighbor coupling are briefly considered. Our world consists largely of networks whose nodes can be neurons (brain), subjects (social networks, ecology), devices (power grids), devices (power grids), and elements (chemical reactions and biological systems). Therefore, in practice, it may be difficult to assign a different coupling or system parameter value to each oscillator in order to enhance the response to a weak external signal. Because of this practical problem, the present paper suggests that an identical coupling may alternatively be used to amplify weak signals in nonlinear physical systems by assigning the same coupling to all oscillators to achieve this task.

Previous studies on the behavior of signals in complex networks have mostly dealt with the case of different coupling or system parameters among the system oscillators (or neurons) [10–12,17–20], whereas the mean field influx density is sufficient for dynamics control in identically coupled systems [21]. This parameter can either promote rhythmogenesis or quench oscillations in coupled Stuart-Landau and Rössler oscillators, van der Pol circuits, spatial ecology, and epidemiology [22–27]. However, the effects of mean field density (including both promoting and inhibiting effects) on resonancelike behavior and weak external periodic signal amplification is still an open question and the subject of the present paper.

*ftndjomatchoua@gmail.com

The present study aims to identify the influence of the mean field density on the signal response in networks of coupled oscillators. Following the literature [10–12,18–20], globally coupled and overdamped bistable oscillators subjected to weak periodic stimuli are taken as a case study. We find that the signal response exhibits a clear maximum at an optimal level of mean field density. Remarkably, the bell-shaped signal response curves produced are comparable to the weak signal response in the diversity models in the literature. Through an analytical approach, it is shown that during the collective oscillation, this resonancelike phenomenon is driven by the nonmonotonic change in the height of the barrier and the bistability character of the effective potential energy. Finally, the robustness of this phenomenon to various signal waveforms is examined.

II. THE MODEL

The main model used in this study is a mean field (all-to-all) coupled overdamped and bistable oscillators [10–12,18–20],

$$\dot{x}_i = x_i - x_i^3 + \frac{C}{N} \sum_{j=1}^N (\alpha x_j - x_i) + f \sin(\omega t), \quad (1)$$

where $i = 1, \dots, N$, f is the amplitude of external signal, ω its frequency, C the coupling strength, and the parameter α controls the influx density of the mean field in the diffusive coupling [21]. In this study, $|\alpha| \leq 1$. This parameter has been extensively applied in many distinct branches of science and engineering to control the dynamics of mean field networked oscillators [21–27]. In the limit of $\alpha = 0$, the oscillators are decoupled and modified with an additional self-feedback term. The case of $\alpha = 1$ corresponds to the full mean field diffusion. For decreasing α from 1 to -1 , the mean field effect in the coupling is gradually weakened [21–27].

III. SIGNAL AMPLIFICATION

Without coupling ($C = 0$) and an external signal ($f = 0$), Eq. (1) represents a single bistable oscillator which has a double-well potential $V(x) = -x^2/2 + x^4/4$ with two bottoms centered around $x^* = \pm 1$, provided there are two types of stable oscillations. For a weak external signal, i.e., $f < f_{\text{th}}$, depending on the starting state, the oscillator wiggles a little at the bottom of one of the two wells. For a strong external signal, i.e., $f > f_{\text{th}}$, the oscillator moves with a considerable amplitude by switching back and forth between the two wells. The threshold of the amplitude of the external signal is $f_{\text{th}} = \sqrt{4/27} \simeq 0.3849$ [10–12,28]. Throughout this paper, the parameters considered are $N = 50$, $\omega = 0.1$, $C = 1$, and $f = 0.1 < f_{\text{th}}$. Under this weak signal, the oscillators in Eq. (1) cannot switch between their two wells at $C = 0$. to be a subthreshold, i.e., it does not suffice to induce the oscillators to jump between the two minima in any additional force. The numerical calculations are implemented through the fifth-order Runge-Kutta method with a fixed time step $\Delta t = 0.01$, and the initial conditions of the units are randomly chosen from the two fixed points $x^* = \pm 1$ [10,12,18–20].

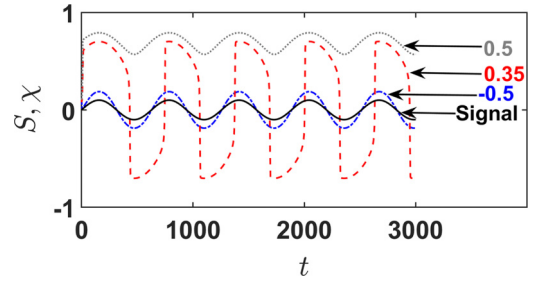


FIG. 1. Signal amplification by different values of the mean field density. The average system response is $\chi(t) = N^{-1} \sum_{i=1}^N x_i$, for $\alpha = -0.5$ (blue), 0.35 (red), and 0.5 (gray), and the input signal $S(t) = f \sin(\omega t)$ in black. The parameters used are $f = 0.1$, $\omega = 0.1$, $N = 50$, and $C = 1$.

The average value $\chi(t) = N^{-1} \sum_{i=1}^N x_i$ is considered as the representative response of the system [10,12,18–20].

The optimal amplification of the input signal as a function of α can clearly be observed in Fig. 1 which shows representative trajectories for $\alpha = -0.5$ (small oscillations around the value $\chi = 0$), $\alpha = 0.35$ (large oscillations between $\chi \simeq +1$ and $\chi \simeq -1$), and $\alpha = +0.5$ (small oscillations near $\chi = +1$). This result suggests that there is an intermediate (critical) value for which the system responds optimally. The mechanism underlying this resonancelike behavior is further analyzed in the following section.

IV. CRITICAL MEAN FIELD DENSITY

In the previous section, it is shown that the variation of the parameter α is sufficient for increasing the response of the system. Note that the summation term in Eq. (1) can be rewritten as

$$\frac{C}{N} \sum_{j=1}^N (\alpha x_j - x_i) = C(\alpha \chi - x_i). \quad (2)$$

The insertion of Eq. (2) into Eq. (1) yields

$$\dot{x}_i = x_i - x_i^3 + C(\alpha \chi - x_i) + f \sin(\omega t). \quad (3)$$

By taking the average of the left-hand-side term of Eq. (3) as well as all the right-hand term of the same equation, the following equation is obtained,

$$\dot{\chi} = \gamma \chi - \frac{1}{N} \sum_{i=1}^N x_i^3 + f \sin(\omega t), \quad (4)$$

where the parameter γ is defined by $\gamma = 1 - C(1 - \alpha)$.

Following Refs. [10,11], the quantity $\delta_i = x_i - \chi$ is introduced to represent the trajectory deviation between x_i and the average activity of the system χ . After development, $N^{-1} \sum_{i=1}^N x_i^3 = \chi^3 + 3M_2 \chi + 3M_1 \chi^2 + M_3$, with $M_1 = \sum_{i=1}^N \delta_i$, $M_2 = \sum_{i=1}^N \delta_i^2$, and $M_3 = \sum_{i=1}^N \delta_i^3$. Under the assumption of a high degree of synchronization between the unit oscillator, an average activity $M_1 \simeq 0$, $M_3 \simeq 0$. Furthermore, M_2 vanishes after an initial transient washes out the effect of possible different initial x_i conditions [11]. The ensemble dynamics can be therefore translated into

$$\dot{\chi} = \gamma \chi - \chi^3 + f \sin(\omega t). \quad (5)$$

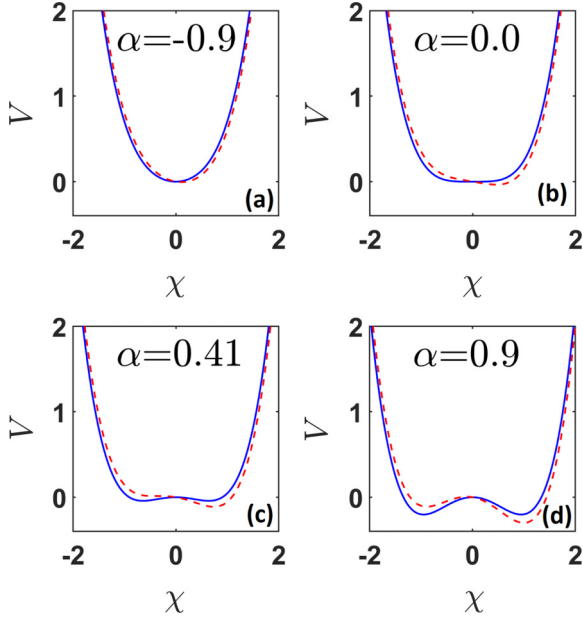


FIG. 2. The potential of Eq. (7) for (a) $\alpha = -0.9$, (b) $\alpha = 0$, (c) $\alpha = 0.41$, and (d) $\alpha = +0.9$. Solid and dashed lines denote the potential at $t = 0$ and $t = \pi/(2\omega)$. The parameters used are the same in Fig. 1.

This equation describes the overdamped motion of a *particle* in a coupling-dependent potential with a periodic force. Adding the signal to the potential, we get the potential energy

$$V(\chi, t) = \frac{\chi^4}{4} - \frac{\gamma\chi^2}{2} - \chi f \sin(\omega t). \quad (6)$$

Since the signal amplitude f is fixed, the magnitude of mean field density α becomes important to the potential V . The dependences of V on α at $t = 0$ and $t = \pi/(2\omega)$ are illustrated in Fig. 2. For $\alpha = -0.9$, the potential V is \mathbf{V} shaped with a single well and χ is highly confined [Fig. 2(a)]. With the increases of α , V turns progressively into a \mathbf{U} -shaped potential and the confinement reduces as the bottom of the well becomes larger [Fig. 2(b)]. The oscillatory motions are stable around the equilibrium but with a larger amplitude. When α reaches $\alpha_1 = 0.40$ [Fig. 2(c)], a two-well configuration appears with a slight barrier (\mathbf{W} -shaped potential). The potential barriers vanish when the external signal arrives at its maximum or minimum, and the particle can pass over the barriers. For $\alpha = 0.9$, the potential barrier becomes higher. As t evolves, the two barriers periodically rise and fall but maintain the well [Fig. 2(d)]. In this case the particle cannot pass over the barriers if it is initially in the potential well. For $\alpha < 0.41$ the external signal is a suprathreshold which can force the particle out of the potential well, and thus $\alpha_1 = 0.41$ is the approximative critical mean field density strength.

The switching between the two wells becomes possible when the bistability of the potential is destroyed [19,20,28]. The condition for this to happen is given by the condition that the cubic equation $\gamma\chi - \chi^3 + f = 0$ have three real roots [19,20,28]. Therefore, the necessary condition for the

discriminant is $(f/2)^2 - (\gamma/3)^3 = 0$, which gives

$$\alpha_{cr} = \frac{C-1}{C} + \frac{3}{C} \left(\frac{f}{2} \right)^{\frac{2}{3}}. \quad (7)$$

For $f = 0.1$ in Eq. (7), the critical mean field density strength is given by $\alpha_{cr} \simeq 0.4072$, which is in good agreement with the numerical result $\alpha_1 \simeq 0.41$. In our amplification point of view, the only dynamical events are well-to-well switching transitions, and these occur whenever $\alpha < \alpha_{cr}$. This resonance is thus fundamentally a threshold phenomenon.

V. SPECTRAL AMPLIFICATION

A. Numerical analysis

To evaluate the amplitude of the input frequency in the output signal, we calculate the Fourier coefficient η for the input frequency ω . We use the η parameter instead of the power spectrum because we are interested in the information encoded in the frequency ω . For this task the η parameter is a much more compact tool than the power spectrum [10–12,17–20]. The spectral amplification is computed as follows: $\eta = Q/f$,

$$Q = |\langle \exp(i\omega t) \chi(t) \rangle| \\ = \frac{2}{MT} \left| \int_{t_0}^{t_0+MT} \chi(t) [\cos(\omega t) + i \sin(\omega t)] dt \right|, \quad (8)$$

$i^2 = -1$, $|\dots|$ the complex modulus, and $\langle \dots \rangle$ the time averaging. In our simulation we take $M = 50$ and t_0 sufficiently long to remove transient dynamics. The integrals in Eq. (8) are evaluated numerically through the Simpson's algorithm [29]. The initial conditions are taken sufficiently near to 0 during the numerical estimate of η [13].

B. Theoretical analysis

To find an approximative analytical solution to Eq. (5), linear and nonlinear approaches are used.

The linear approach consists in introducing a perturbation $\varepsilon(t)$ to $\chi(t)$ around the equilibrium point χ_{eq} (with $f = 0$). The obtained linearized differential equation is

$$\dot{\varepsilon} = [1 - C(1 - \alpha) - 3\chi_{eq}^2] \varepsilon + f \sin(\omega t), \quad (9)$$

with

$$\chi_{eq} = \begin{cases} \chi_{eq}^{\pm} = \pm \sqrt{1 - C(1 - \alpha)}, & \alpha < \alpha_{cr}^*, \\ \chi_{eq}^0 = 0, & \alpha \geq \alpha_{cr}^*, \end{cases} \quad (10)$$

where $\alpha_{cr}^* = \alpha_{cr}$ obtained from Eq. (7) when $f = 0$. The solution of Eq. (5) in the linear framework is

$$\chi(t) = \begin{cases} \chi_{eq}^{\pm} + \frac{f \sin(\omega t + \phi_2)}{\sqrt{\omega^2 + 4[1 - C(1 - \alpha)]^2}}, & \alpha < \alpha_{cr}^*, \\ \chi_{eq}^0 + \frac{f \sin(\omega t + \phi_1)}{\sqrt{\omega^2 + [1 - C(1 - \alpha)]^2}}, & \alpha \geq \alpha_{cr}^*, \end{cases} \quad (11)$$

with the phase shift $\phi_2 = \tan^{-1}\{-\omega/2[1 - C(1 - \alpha)]\}$, $\phi_1 = \tan^{-1}\{\omega/[1 - C(1 - \alpha)]\}$. The calculation of the spectral amplification Q/f from the solution Eq. (11) is made by

first computing

$$\begin{aligned} Q &= \sqrt{Q_c^2 + Q_s^2}, \\ Q_c &= \frac{2}{T} \int_{t_0}^{t_0+T} \chi(t) \cos(\omega t) dt, \\ Q_s &= \frac{2}{T} \int_{t_0}^{t_0+T} \chi(t) \sin(\omega t) dt, \end{aligned} \quad (12)$$

which leads to the result

$$\eta = \frac{Q}{f} = \begin{cases} \frac{1}{\sqrt{\omega^2 + 4[1-C(1-\alpha)]^2}}, & \alpha < \alpha_{cr}^*, \\ \frac{1}{\sqrt{\omega^2 + [1-C(1-\alpha)]^2}}, & \alpha \geq \alpha_{cr}^*, \end{cases} \quad (13)$$

with $T = 2\pi/\omega$.

The nonlinear approach consists of finding an approximate analytical value of $\chi(t)$ of Eq. (5) using the harmonic balance method [30], which amounts to seeking $\chi(t)$ in the form

$$\chi(t) = \sum_{n=1}^H a_n \cos(n\omega t) + a_{n+1} \sin(n\omega t), \quad (14)$$

where a_n are the Fourier coefficients and H is the number of harmonics. Inserting Eq. (14) (with $H = 1$) in Eq. (5) and equating the coefficient of the cosine and sine terms separately, one obtains

$$\begin{aligned} 3a_1^3 + 3a_1a_2^2 - 4a_1\gamma + 4a_2\omega &= 0, \\ \frac{3a_1^2a_2}{4} - a_1\omega + \frac{3a_2^3}{4} - a_2\gamma - f &= 0. \end{aligned} \quad (15)$$

Note that $\chi(t) = \mathcal{A} \sin(\omega t + \phi)$, $\mathcal{A} = \sqrt{a_1^2 + a_2^2}$, $\phi = \tan^{-1}(a_2/a_1)$ [30]. After some algebraic manipulations of Eq. (15), the following relationships are obtained:

$$\begin{aligned} \eta &= \frac{\mathcal{A}}{f}, \\ 9\mathcal{A}^6 - 24\gamma\mathcal{A}^4 + 16(\gamma^2 + \omega^2)\mathcal{A}^2 - 16f^2 &= 0. \end{aligned} \quad (16)$$

When $\eta > 1$ the system successfully amplified the signal with the frequency ω , otherwise, the signal decreased. Thus η stands for the *spectral amplification factor*.

C. Resonant amplification from mean field density

In Fig. 3, we plot the amplification factor η versus the mean field density α for the external forcing with an amplitude f below the threshold value. As predicted, there is an optimum value of the mean field density for maximum amplification, the main result of this paper. Notice that our approximate treatment agrees rather well with the results coming from a direct numerical integration of the original set of Eq. (1), when the signal is slow. With α near -1 , $\eta \leq 1.0$. The spectral amplification increases up to a maximal value $\eta > 1$ near α_{cr} in a resonancelike manner, and subsequently drops to $\eta < 1$. For $\omega = 0.1$, the maximal spectral amplification is $\eta_{max}^L \simeq 10$, $\eta_{max}^{NL} \simeq 10$, and $\eta_{max}^{num} \simeq 6.367$ where L, NL, and num stand for linear, nonlinear, and numerical, respectively.

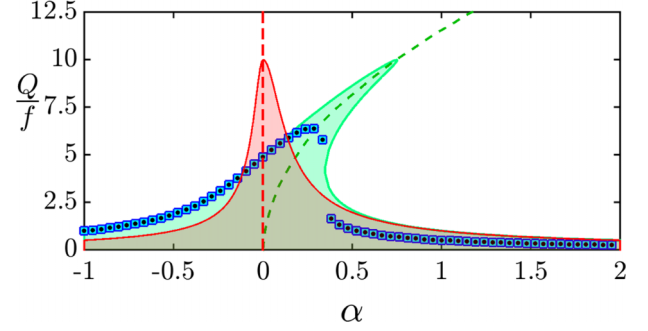


FIG. 3. The spectral amplification factor of the system as a function of the mean field density. The blue colored squares are obtained by numerically solving Eqs. (1) and (8), while the black colored dots are obtained from Eqs. (5) and (8). The theoretical results (linear and nonlinear analysis) are obtained from Eq. (13) (pink area bounded by the red line) and Eq. (16) (green area bounded by the green line), respectively. The dashed line is the resonant backbone for both linear (red color) and nonlinear (green color) cases, respectively. The frequency is $\omega = 0.1$. The remaining parameters used are the same as in Fig. 1.

VI. INFLUENCE OF THE SIGNAL SHAPE ON SIGNAL AMPLIFICATION

In the previous section, it is assumed that the external signal is a periodic sinusoidal function although the majority of signals in nature are more complex than sine waves. In Refs. [12,31], the effect of signal shape on the amplification has been investigated. In what follows, both signal waveform and the mean field density effect are analyzed. It is now assumed that the external signal in Eq. (1) has the form [32]

$$S(r, t) = \frac{f(1-r)^2}{2} \frac{1 - \cos(\omega t)}{1 + r^2 + 2r \cos(\omega t)}. \quad (17)$$

The shape parameter is r ($|r| < 1$), the period $T = 2\pi/\omega$ is the time lag between two consecutive pulses, and f is the amplitude of the driving force $S(r, t)$. This signal may be experimentally implemented by electrical circuits as suggested in Ref. [32].

Figure 4 shows the influence of the shape parameter r on the driving force $S(r, t)$. The force $S(r, t)$ is reduced to a sinusoidal signal when the shape parameter $r = 0$, while for $r > 0$ and $r < 0$, $S(r, t)$ provides respectively broad wells separated by narrow barriers and deep narrow wells separated by broad flat barriers. Note that for $r \rightarrow -1$ the impulse is very wider, whereas for $r \rightarrow +1$ the width of the impulse is

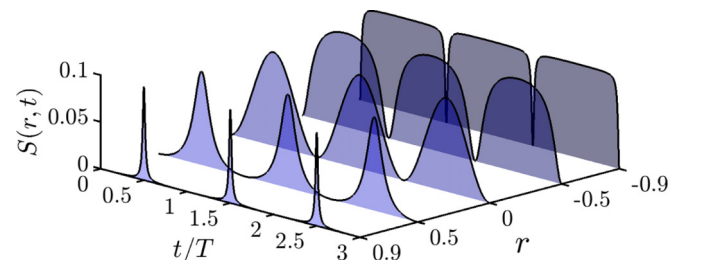


FIG. 4. Influence of the shape parameter r on the driving force $S(r, t)$, for $r = \{-0.9; -0.5; 0; +0.5; +0.9\}$, $f = 0.1$, and $\omega = 0.1$.

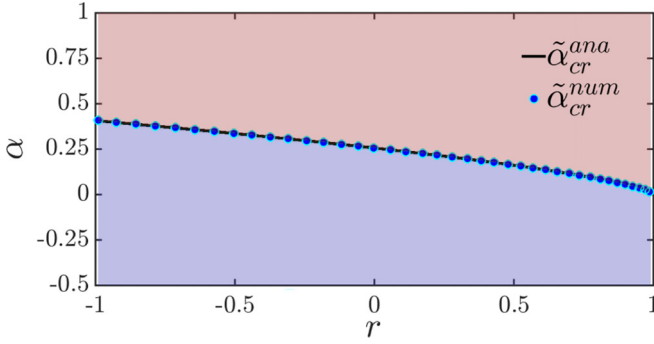


FIG. 5. Influence of the shape parameter r on the critical mean field density $\tilde{\alpha}_{cr}$. The analytical solution $\tilde{\alpha}_{cr}^{ana}$ (black line) is obtained from Eq. (21), while the numerical solution $\tilde{\alpha}_{cr}^{num}$ is obtained by means of Eq. (19) for $\dot{\chi} = 0$, $t = \pi/(2n\omega)$. The critical curve delimits the zone between χ_0^* (blue zone) and $\chi_{1,2}^*$ (pink zone).

narrow. Thus, it would be interesting to study, as in Sec. V, the influence of this deformable force on signal amplification.

$$\chi(t) \approx \begin{cases} \chi_0^* + \sum_{n=1}^{+\infty} \frac{f(1-r^2)(-1)^n r^{n-1} \cos(n\omega t + \phi_{n,0})}{2\sqrt{n^2\omega^2 + [1-C(1-\alpha)-3\chi_0^{*2}]^2}}, & \alpha \leq \tilde{\alpha}_{cr}, \\ \chi_{1,2}^* + \sum_{n=1}^{+\infty} \frac{f(1-r^2)(-1)^n r^{n-1} \cos(n\omega t + \phi_{n,1,2})}{2\sqrt{n^2\omega^2 + [1-C(1-\alpha)-3\chi_{1,2}^{*2}]^2}}, & \alpha > \tilde{\alpha}_{cr}, \end{cases} \quad (20)$$

with

$$\tilde{\alpha}_{cr} = 1 - \frac{1}{C} + \frac{3}{2C} \sqrt{\frac{f^2(1-r)^2}{2}},$$

$$\chi_0^* = \sqrt[3]{\frac{-q + \sqrt{q^2 + \frac{4p^3}{27}}}{2}} + \sqrt[3]{\frac{-q - \sqrt{q^2 + \frac{4p^3}{27}}}{2}}, \quad (21)$$

$$\chi_1^* = 2\sqrt{-\frac{p}{3}} \cos \left[\frac{1}{3} \arccos \left(-\frac{q}{2} \sqrt{-\frac{27}{p^3}} \right) \right],$$

$$\chi_2^* = 2\sqrt{-\frac{p}{3}} \cos \left[\frac{1}{3} \arccos \left(-\frac{q}{2} \sqrt{-\frac{27}{p^3}} \right) + \frac{2\pi}{3} \right], \quad (22)$$

$$\phi_{n,0,1,2} = \arctan \left(\frac{n\omega}{1-C(1-\alpha)-3\chi_{0,1,2}^{*2}} \right),$$

$$p = -1 + C(1-\alpha), \quad q = -\frac{f(1-r)}{2}. \quad (23)$$

Furthermore, we obtain, after using Eq. (12),

$$\eta = \frac{Q}{f} = \begin{cases} \frac{1-r^2}{2\sqrt{\omega^2 + [1-C(1-\alpha)-3\chi_0^{*2}]^2}}, & \alpha \leq \tilde{\alpha}_{cr}, \\ \frac{1-r^2}{2\sqrt{\omega^2 + [1-C(1-\alpha)-3\chi_{1,2}^{*2}]^2}}, & \alpha > \tilde{\alpha}_{cr}. \end{cases} \quad (24)$$

It thus appears that the new critical diversity coefficient $\tilde{\alpha}_{cr}$ depends on the amplitude f of the force and on the shape parameter r as well.

Figure 5 gives the variation of the mean field density as a function of the shape parameter r . In this figure, the blue zone corresponds to a single stable equilibrium χ_0^* , while the

Taking into account the fact that the $S(r, t)$ form is difficult to handle during analytical study, it is transformed through Fourier's series [32]. Thus, the equation governing the dynamics of the coupled system is

$$\dot{x}_i = x_i - x_i^3 + \frac{C}{N} \sum_{j=1}^N (\alpha x_j - x_i) + \frac{f(1-r)}{2} + \frac{f(1-r^2)}{2} \sum_{n=1}^{+\infty} (-1)^n r^{n-1} \cos(n\omega t), \quad (18)$$

and the averaged equation is

$$\dot{\chi} = [1 - C(1-\alpha)]\chi - \chi^3 + \frac{f(1-r)}{2} + \frac{f(1-r^2)}{2} \sum_{n=1}^{+\infty} (-1)^n r^{n-1} \cos(n\omega t). \quad (19)$$

According to the analysis made in Sec. VB, the approximate solution of Eq. (19) is given by

pink zone corresponds to two stable equilibria states $\chi_{1,2}^*$. The analytical solution $\tilde{\alpha}_{cr}^{ana}$ (black line) is obtained from Eq. (21), while the numerical solution $\tilde{\alpha}_{cr}^{num}$ is obtained from Eq. (19) for $\dot{\chi} = 0$, $t = \pi/(2n\omega)$.

Figure 6 shows the influence of the shape parameter r and the mean field density on the signal amplification. As observed in Fig. 6(a), η increases and reaches a maximum value when $\alpha \leq \tilde{\alpha}_{cr,i}$, $i = 1, 2, 3$. On the other hand, when $\alpha > \tilde{\alpha}_{cr,i}$, $i = 1, 2, 3$, a decrease in η is observed. Figure 6(b) gives a comparison between the numerical and analytical investigation for the signal amplification. Note that the analytical investigation is conducted by solving the system:

$$\frac{\omega}{\pi} \int_0^{\frac{2\pi}{\omega}} \mathcal{E}(t, a_1, a_2) \cos(\omega t) dt = 0, \quad (25)$$

$$\frac{\omega}{\pi} \int_0^{\frac{2\pi}{\omega}} \mathcal{E}(t, a_1, a_2) \sin(\omega t) dt = 0,$$

by means of the Newton-Raphson method coupled with the Simpson's algorithm, and the nonlinear function $\mathcal{E}(t, a_1, a_2)$ is defined by

$$\mathcal{E} = \omega[-a_1 \sin(\omega t) + a_2 \cos(\omega t)] - [1 - C(1-\alpha)] \times [a_1 \cos(\omega t) + a_2 \sin(\omega t)] + [a_1 \cos(\omega t) + a_2 \sin(\omega t)]^3 - \frac{f}{2}(1-r)^2 \frac{1 - \cos(\omega t)}{1 + r^2 + 2r \cos(\omega t)}. \quad (26)$$

Once the unknowns a_1 and a_2 are determined, the amplification coefficient is calculated as in Sec. VB. As observed in Fig. 6(b), the numerical solution [yellow/blue colored squares

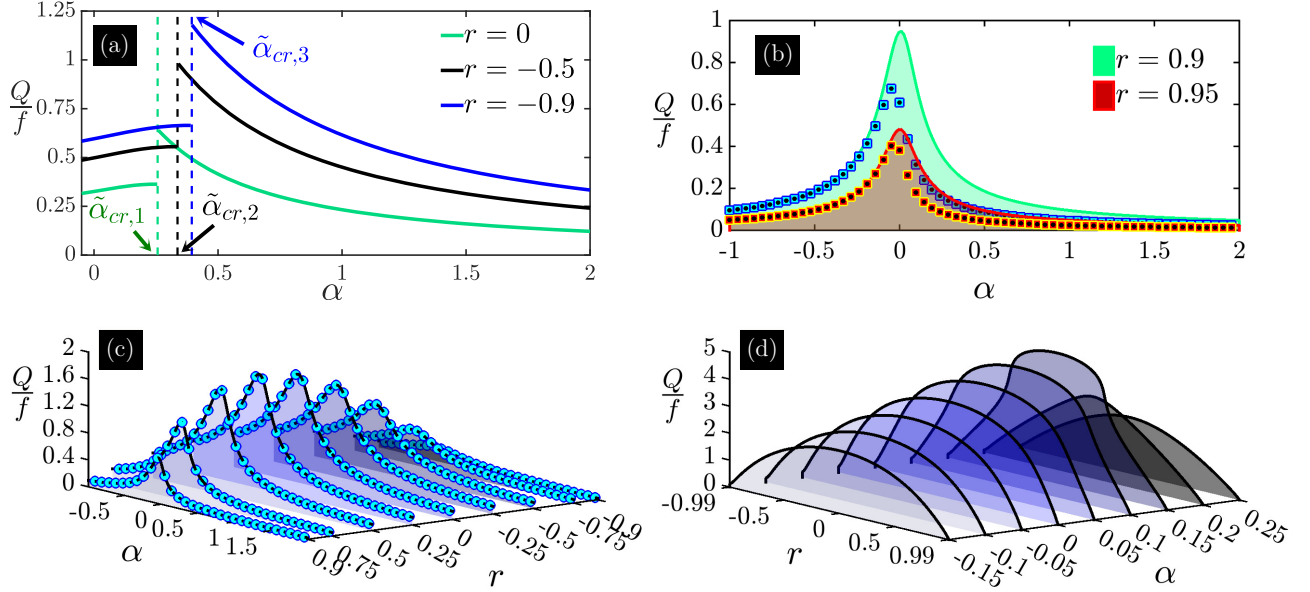


FIG. 6. Influence of the shape parameter r and the mean field density α on the signal amplification in the case of linear approximation [(a) with $\tilde{\alpha}_{cr,1} \approx 0.256446807822$, $\tilde{\alpha}_{cr,2} \approx 0.336644071523$, and $\tilde{\alpha}_{cr,3} \approx 0.394187918494$]. (b) obtained for $r = 0.9$ and $r = 0.95$. The red and green colored lines come from Eq. (21), while the yellow and blue colored squares, as well as the black colored dots, are the solutions of Eqs. (18) and (19), respectively. The simultaneous effect of r and α on η is highlighted in (c) [using Eq. (18) (black colored lines) and Eq. (19) (blue colored circles)] and (d) [using Eq. (25)]. For all these panels, ω is set to $\omega = 0.1$ and the remaining parameters used are the same as in Fig. 1.

and black colored dots, obtained using Eqs. (18) and (19), respectively] coincides with the analytical solution given by Eq. (25) (red/green colored line) for $r = 0.9$ and $r = 0.95$. Figure 6(c) gives a perfect match between the signal amplification coefficient, the 50 coupled units (black colored lines), and the mean equation (blue colored circles) when the shape parameter r and the mean field density vary simultaneously. The same observation is noticed for Fig. 6(d) obtained from Eq. (25). It follows from Fig. 6 that the shape of the signal $S(r, t)$ also plays a significant role in the amplification of the system response.

VII. INFLUENCE OF THE NETWORK TOPOLOGY ON SIGNAL AMPLIFICATION

The aim here is to investigate whether a resonantlike the signal amplification still occurs when the coupling between the network units changes. For this purpose, the nearest-neighbor coupling,

$$\dot{x}_i = x_i - x_i^3 + \frac{C}{2}(\alpha x_{i+1} - x_i) + \frac{C}{2}(\alpha x_{i-1} - x_i) + S(t), \quad (27)$$

as well as the starlike coupling [33],

$$\dot{x} = x - x^3 + \frac{C}{N} \sum_{j=1}^N (\alpha x_j - x) + S(t),$$

$$\dot{x}_j = x_j - x_j^3 + C(\alpha x_j - x) + S(t), \quad j = 1, 2, \dots, N, \quad (28)$$

are used, where $S(t)$ can be a sinusoidal function [$S(t) = f \sin(\omega t)$] or a deformable periodic function defined in Eq. (17). Given the form of Eqs. (27) and (28), the response of the system is obtained through numerical and

semianalytical methods. Note that the numerical simulation is done with periodic boundary conditions when necessary. The semianalytical method is based on Eq. (25) with the variables a_1, a_2 and the nonlinear function $\mathcal{E}(t, a_1, a_2)$ which now depends on the number of units [$a_1 \rightarrow a_{i,1}$, $a_2 \rightarrow a_{i,2}$, $\mathcal{E}(t, a_1, a_2) \rightarrow \mathcal{E}_i(t, a_{i,1}, a_{i,2})$, $\eta = \frac{1}{Nf} \sqrt{\sum_{i=1}^N (a_{i,1}^2 + a_{i,2}^2)}$, $i = 1, 2, \dots, N$]. Let us specify that the nonlinear function $\mathcal{E}_i(t, a_{i,1}, a_{i,2})$ is obtained by looking for a solution under the form $x_i(t) = a_{i,1} \cos(\omega t) + a_{i,2} \sin(\omega t)$. The solution is further introduced in Eq. (27).

Figure 7 shows the influence of the system topology on the signal amplification. As observed in Figs. 7(a) and 7(b), the nearest-neighbor coupling gives qualitatively similar results compared to all-to-all coupling studied in Sec. V. However, when the coupling topology is of the star type, the amplification of the system exhibits a double-resonance peak [see Figs. 7(c) and 7(d) for the sinusoidal and deformable function, respectively] obtained for positive values of the mean field density α . This result shows that the starlike coupling between the network units not only influences the shape of the system response but also contributes to the maximum amplification compared to the cases of all-to-all and nearest-neighbor coupling cases.

VIII. DISCUSSION AND CONCLUSION

It is well known that mean field density (MFD) plays constructive roles in many coupled systems [21]. For example, this parameter can either promote rhythmogenesis or quench oscillations in coupled Stuart-Landau and Rössler oscillators, van der Pol electrical circuits, spatial ecology, and epidemiology [22–27]. Our findings here show that natural systems

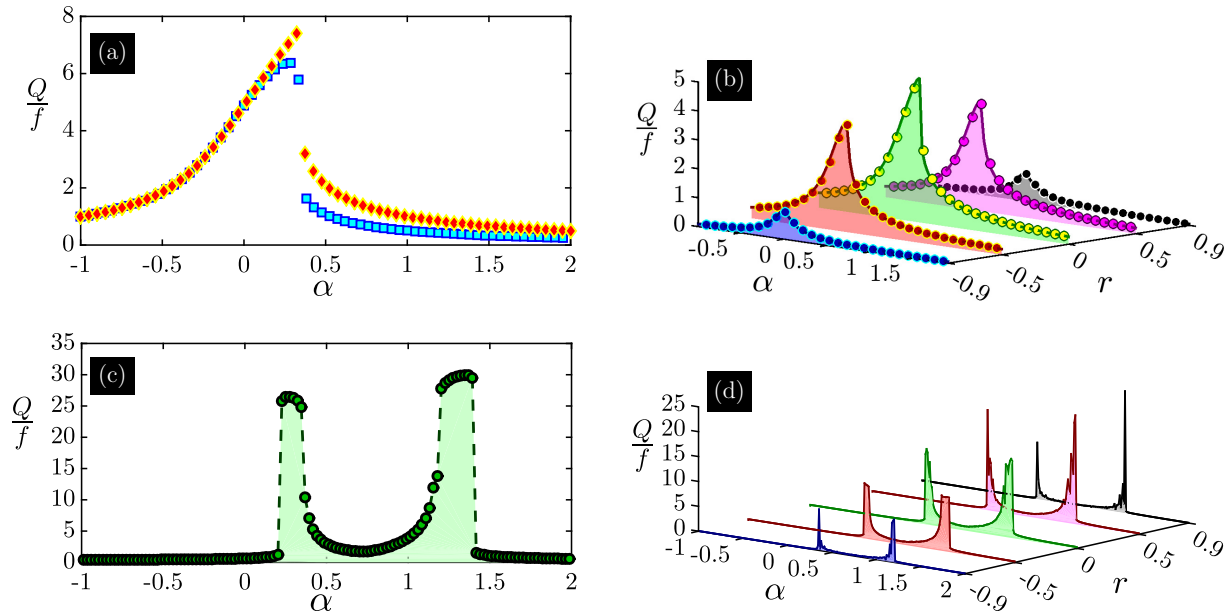


FIG. 7. Signal amplification as a function of mean field density α and shape parameter r for next-nearest-neighbor coupling [(a) and (b)] and starlike network coupling [(c) and (d)]. (a) Comparison between numerical simulation of Eq. (27) (solid red diamonds) and semianalytical one (solid blue square) when $S(t)$ is a sinusoidal function. (b) Three-dimensional graph comparing semianalytical solutions obtained with all-to-all coupling (solid lines) and next-nearest-neighbor coupling (solid circles) for different shape parameter values. Amplification from the numerical simulation of Eq. (28) obtained with a sinusoidal function [(c)] and a deformable one [(d)] for starlike coupling. For all these panels, ω is set to $\omega = 0.1$ and the remaining parameters used are the same as in Fig. 1.

might profit from the MFD in order to optimize the response to an external stimulus.

The mainstream idea in optimizing globally coupled oscillator response is based on optimal heterogeneity [7–14,16–20], whereas the current study shows that it is possible to achieve the same result in a homogeneous network model simply by changing the MFD. Therefore, such constructive effects of MFD in complex systems may deserve more and more attention in future works.

We have examined the signal response of connected bistable oscillators to mean field density variations in networks. We provide an intriguing type of MFD-enhanced signal response to external periodic stimulation that is resilient

to density and network size through extensive numerical simulations. This kind of MFD-enhanced signal response to periodic external forcing is crucial to the system’s overall response. In addition, we performed a simple mean field analysis that can qualitatively match the outcomes of the simulation. Our research might be very helpful in understanding how other networked systems can respond collectively to external signals when MFD is present. One research area that attracts the attention of scientists working on complex networks is signal propagation [34–36]. This important aspect is an interesting avenue for future investigation to test how an enhanced signal response affects signal transport from one node to another [34–36].

[1] F. Moss, M. W. Lawrence, and G. S. Walter, Stochastic resonance and sensory information processing: A tutorial and review of application, *Clin. Neurophysiol.* **115**, 267 (2004).

[2] Z. Qiao, Y. Lei, and N. Li, Applications of stochastic resonance to machinery fault detection: A review and tutorial, *Mech. Syst. Signal Process.* **122**, 502 (2019).

[3] R. Vijay, M. H. Devoret, and I. Siddiqi, Invited review article: The Josephson bifurcation amplifier, *Rev. Sci. Instrum.* **80**, 111101 (2009).

[4] M. L. Ku, W. Li, Y. Chen, K. Ray, and J. Liu, Advances in energy harvesting communications: Past, present, and future challenges, *IEEE Commun. Surv. Tutor.* **18**, 1384 (2016).

[5] W. Chen, K. M. Beck, R. Bicker, M. Gullans, M. D. Lukin, H. Tanji-Suzuki *et al.*, All-optical switch and transistor gated by one stored photon, *Science* **341**, 768 (2013).

[6] M. Malishava and R. Khomeriki, All-Phononic Digital Transistor on the Basis of Gap-Soliton Dynamics in an Anharmonic Oscillator Ladder, *Phys. Rev. Lett.* **115**, 104301 (2015).

[7] S. Rajasekar and M. A. F. Sanjuan, *Nonlinear Resonances* (Springer, Berlin, 2016).

[8] D. Chevriaux, R. Khomeriki, and J. Leon, Theory of a Josephson junction parallel array detector sensitive to very weak signals, *Phys. Rev. B* **73**, 214516 (2006).

[9] A. Valizadeh, Enhanced response of regular networks to local signals in the presence of a fast impurity, *Phys. Rev. E* **86**, 016101 (2012).

[10] C. Liu, C. Y. Wang, Z. X. Wu, H. X. Yang, and J. Y. Guan, Diversity-induced resonance in a globally coupled bistable system with diversely distributed heterogeneity, *Chaos* **32**, 083112 (2022).

- [11] C. J. Tessone, C. R. Mirasso, R. Toral, and J. D. Gunton, Diversity-Induced Resonance, *Phys. Rev. Lett.* **97**, 194101 (2006).
- [12] X. Liang and X. Zhang, Signal amplification enhanced by large phase disorder in coupled bistable units, *Phys. Rev. E* **104**, 034204 (2021).
- [13] K. Abirami, S. Rajasekar, and M. A. F. Sanjuan, Vibrational and ghost-vibrational resonances in a modified chua's circuit model equation, *Int. J. Bifurcation Chaos* **24**, 1430031 (2014).
- [14] M. V. Tchakui, P. Wofo, and P. Colet, Signal bi-amplification in networks of unidirectionally coupled MEMS, *Eur. Phys. J. B* **89**, 22 (2016).
- [15] X. Liang, M. Tang, and H. Lü, Signal transmission in a Y-shaped one-way chain, *Chaos* **23**, 043113 (2013).
- [16] S. Rajamani and S. Rajasekar, Signal amplification by unidirectional coupling of oscillators, *Phys. Scr.* **88**, 015010 (2013).
- [17] J. A. Acebrón, S. Lozano, and A. Arenas, Amplified Signal Response in Scale-Free Networks by Collaborative Signaling, *Phys. Rev. Lett.* **99**, 128701 (2007).
- [18] T. Vaz Martins, V. N. Livina, A. P. Majtey, and R. Toral, Resonance induced by repulsive interactions in a model of globally coupled bistable systems, *Phys. Rev. E* **81**, 041103 (2010).
- [19] C. Liu and X. Liang, Resonance induced by coupling diversity in globally coupled bistable oscillators, *Phys. Rev. E* **100**, 032206 (2019).
- [20] X. Liang, C. Liu, and X. Zhang, Positive and negative couplings perform complementary roles in the signal amplification of globally coupled bistable oscillators, *Phys. Rev. E* **101**, 022205 (2020).
- [21] W. Zou, D. V. Senthilkumar, M. Zhan, and J. Kurths, Quenching, aging, and reviving in coupled dynamical networks, *Phys. Rep.* **931**, 1 (2021).
- [22] T. Banerjee and D. Ghosh, Experimental observation of a transition from amplitude to oscillation death in coupled oscillators, *Phys. Rev. E* **89**, 062902 (2014).
- [23] A. Sharma and M. D. Shrimali, Amplitude death with mean-field diffusion, *Phys. Rev. E* **85**, 057204 (2012).
- [24] T. Banerjee and D. Ghosh, Transition from amplitude to oscillation death under mean-field diffusive coupling, *Phys. Rev. E* **89**, 052912 (2014).
- [25] D. Ghosh, T. Banerjee, and J. Kurths, Revival of oscillation from mean-field-induced death: Theory and experiment, *Phys. Rev. E* **92**, 052908 (2015).
- [26] T. Banerjee, P. S. Dutta, and A. Gupta, Mean-field dispersion-induced spatial synchrony, oscillation and amplitude death, and temporal stability in an ecological model, *Phys. Rev. E* **91**, 052919 (2015).
- [27] T. Verma and A. K. Gupta, Network synchronization, stability and rhythmic processes in a diffusive mean-field coupled SEIR model, *Commun. Nonlinear Sci. Numer. Simul.* **102**, 105927 (2021).
- [28] F. Moss, D. Pierson, and D. O'Gorman, Stochastic resonance: Tutorial and update, *Int. J. Bifurcation Chaos* **04**, 1383 (1994).
- [29] W. H. Press, S. A. Teukolsky, W. T. Vetterling, and B. P. Flannery, *Numerical Recipes in Fortran: The Art of Scientific Computing*, 2nd ed. (Cambridge University Press, Cambridge, UK, 1992).
- [30] M. Krack and J. Gross, *Harmonic Balance for Nonlinear Vibration Problems* (Springer, Berlin, 2019).
- [31] P. J. Martínez and R. Chacon, Impulse-induced optimum signal amplification in scale-free networks, *Phys. Rev. E* **93**, 042311 (2016).
- [32] F. T. Ndjomatchoua, T. L. M. Djomo, F. F. Kemwoue, C. L. Gninanzlong, M. P. Kepnang, M. S. Siewe *et al.*, Amplitude response, Melnikov's criteria, and chaos occurrence in a Duffing's system subjected to an external periodic excitation with a variable shape, *Chaos* **32**, 083144 (2022).
- [33] S. Gao, N. Gao, B. Kan, and H. Wang, Stochastic resonance in a coupled star-networks with power-law heterogeneity, *Physica A* **580**, 126155 (2021).
- [34] X. Bao, Q. Hu, P. Ji, W. Lin, J. Kurths, and J. Nagler, Impact of basic network motifs on the collective response to perturbations, *Nat. Commun.* **13**, 5301 (2022).
- [35] P. Ji, W. Lin, and J. Kurths, Asymptotic scaling describing signal propagation in complex networks, *Nat. Phys.* **16**, 1082 (2020).
- [36] P. Ji, J. Ye, Y. Mu, W. Lin, Y. Tian, C. Hens, M. Perc, Y. Tang, J. Sun, and J. Kurths, Signal propagation in complex networks, *Phys. Rep.* **1017**, 1 (2023).